3D printed permeation module to monitor interaction of cell membrane transporters with exogenic compounds in real-time

Hana Sklenářová[1*], Michaela Rosecká[1], Burkhard Horstkotte[1], Petr Pávek[2], Manuel Miró[1,3], Petr Solich[1]

[1] Department of Analytical Chemistry, Faculty of Pharmacy in Hradec Králové, Charles University, Akademika Heyrovského 1203, 500 05 Hradec Králové, Czech Republic

[2] Department of Pharmacology and Toxicology, Faculty of Pharmacy in Hradec Králové, Charles University, Akademika Heyrovského 1203, 500 05 Hradec Králové, Czech Republic

[3] FI-TRACE group, Department of Chemistry, University of Balearic Islands, Carretera de Valldemossa km 7.5, 07122 Palma de Mallorca, Spain

Abstract

A new design of 3D printed permeation module was developed to monitor the interaction of exogenic compounds with cell membrane transporters in real-time. The fluorescent marker Rhodamine 123 (Rho123) was applied as a substrate to study the activity of the P-glycoprotein membrane transporter using the MDCKII-MDR1 genetically modified cell line. In addition, the inhibitory effect of verapamil (Ver), a prototype P-glycoprotein inhibitor, was examined in the module, demonstrating an enhanced Rho123 accumulation into cells as well as the applicability of the module for P-glycoprotein inhibitors testing. Inhibition was demonstrated for different ratios of Rho123 and Ver, and their competition in terms of interaction with the P-glycoprotein transporter was monitored in real-time. Employing the 3D-printed module, permeation testing was shortened from 8 h in the conventional module to 2 h and evaluation based on kinetic profiles in every 10 min was possible in both donor and acceptor compartments. We also show that monitoring Rho123 levels in both compartments enables calculate the amount of Rho123 accumulated inside cells without the need of cell lysis.

Keywords

3D printing; Cell membrane transporter; P-glycoprotein; Permeation; Real-time monitoring; Sequential injection analysis

1. Introduction

Permeation studies based on plastic semipermeable membrane supports are widely-used tools in biomedicine to gain a better understanding of the transport of xenobiotics and pharmaceuticals into cells or through different biological barriers such as intestine or skin [1]-[2]. Semipermeable membrane supports or inserts (Fig. 1) made of polycarbonate, polyester, or collagen-coated polytetrafluoroethylene are used as scaffolds for cultivated intestinal epithelial cells as an intact monolayer (such as Caco-2, a cellular model of human intestinal absorption), for brain microvascular endothelial cells, for dermal keratinocyte cells (cellular skin permeation model) or for genetically modified epithelial cells expressing membrane transporters such as MDCKII of LLC-PK1 cells [3]-[5]. The latter application attracted enormous attention of scientists over the last 20 years, which is mainly connected with the expanding knowledge of transporters and their roles in drug absorption and pharmacokinetics or in drug toxicology [6][5]. The importance of such studies is reflected by drug regulatory authorities including the Food and Drug Administration (FDA) or the European Medicine Agency (EMA) that incorporated permeation studies in semipermeable membrane supports into their guidelines [7]-[8].

In the above studies, the permeation of a specific substrate or "tracer" that is initially contained in the cultivation medium of the donor compartment is permeated. From here, it permeates through the cellular membrane into the cultivation medium of the acceptor compartment. A single measurement at the end of the experiment lasting typically 6-8 h or just a few measurements during the permeation process are usually applied in standard protocols of permeation assays with manual sampling of cultivation media from both acceptor and donor compartments.

P-glycoprotein 1 (P-gly) is one of the most important membrane transporters [9], which pumps foreign substances out of cells. P-gly is extensively distributed in the intestinal epithelium where it pumps xenobiotics back into the intestinal lumen or in the blood-brain barrier where it protects the brain against toxic injury. Therefore, inhibitors of P-gly can substantially modify the absorption or distribution of co-administered drugs, which may result in serious toxicological or pharmacological consequences (drug-drug interactions) [10]. Very recently, the FDA focused on testing interactions with P-gly in detail in a draft guideline [8]. An inhibitor of P-gly present in the donor compartment would cause a significant increase of the permeation of a given tracer due to the inhibition of the P-gly-mediated reverse transport

[2] (Fig. 1). This simple experimental approach is usually performed using an off-line format with a single or several few measurements after sampling from semipermeable supports. Unfortunately, the standard approach is laborious and does not allow for fast and continuous (real-time) monitoring of the substrate permeation.

A significant increase in speed, experimental reliability, and gain in information on the kinetics of the transporter inhibition is achieved if automation tools, mostly flow approaches, are employed to enable semi-continuous sampling from the acceptor compartment as we have recently demonstrated [11]. Flow approaches have also been used to automate pharmacopoeial testing of drug dissolution and liberation studies for which glass Franz cells (or chambers) with donor and acceptor/receptor parts are most often applied [12]-[17]. Their design and fabrication materials are steadily being improved, and liberation chambers as well as complete permeation systems are commercially available in various formats including in-line Franz cell modules [18].

A general drawback of previous experiments of real-time permeation monitoring for cell transporter studies using commercial Franz cells was that very low concentrations of the used tracers were found in the acceptor compartment and that the concentration change in the donor compartment was not evaluated. This can be a source of uncertainty because a larger error of measurement is expected at lower tracer concentration unless preconcentration of the tracer from the sample is undertaken before measurement. An important systematic error is that the previous setups cannot provide insight into the extent to which the cells themselves can act as reservoirs for the tracer (in-cell accumulation). Detailed information of the tracer concentration in both donor and acceptor compartments would therefore aid to a deeper understanding of the involved processes on cellular or molecular levels in real-time. Several examples how to solve this problem have been already published. For example, a multi-chamber microfluidic platform to automate multiple permeation studies across full-thickness skin organotypic culture has been described. Skin permeation was tested using a microfluidic array composed of dynamic permeation units moved on top of the 96-well plate where fractions at the respective sampling intervals were collected. The main aim of this study was miniaturization, high throughput, and cost effectiveness of standard tests [2]. Another example encompasses a dynamic model of the intestinal barrier for oral bioavailability studies that was coupled to chip-based LC-MS using the commercial Transwell® inserts with continuous flow in both the apical and the basolateral compartments [19]. A last example of semipermeable (Transwell®) membrane supports involved evaluating *in-vitro* cytotoxicity of nanomaterials in

real-time by a highly sensitive and in situ method for detection of hydrogen peroxide released from several adherent cells [20].

In the development of improved analytical instrumentation and accessories, 3D printing has recently gained major attention in analytical chemistry as a rapid, economic, and perfectly reproducible prototyping and fabrication technique for open and close geometry objects [21] as visualized by the papers compiled in this Virtual Special Issue of ACA. 3D printing has revolutionized the way that micro/millifluidic platforms [22], sensors and biosensing devices [23], sorbent materials [24]-[25], and column separation systems [26]-[27] are fabricated using computer-aided-design and fast iterative changes. For example, in the field of flow injection analysis, an all-included one-step 3D printed Lab-on-Valve platform that accommodates automatic multifarious unit operations and on-valve optical and electrochemical detection [28] served to launch the so-called 3D-μFIA concept. However, little attention to the coupling of 3D printing to analytical toxicology has been paid to date.

The incorporation of membrane-based separation including (micro)dialysis, gas diffusion, filtration and in-vitro permeation tests in 3D printed millifluidic structures or flow injection systems using either commercially available membranes or 3D printed barriers has been reviewed by us [24]. In the context of our work, the seminal papers by Spence's group [29]-[30] using Transwell® inserts without and with immobilized cell monolayers in flow-through 3D printed platforms with multiple tests for drug transport, cell viability and release of ATP from flowing erythrocytes are worth mentioning.

Out of the several 3D printing technologies, namely, fused deposition modelling (FDM), dynamic light processing, stereolithography (SLA), selective laser sintering and photopolymer inkjet printing, the interest on the SLA has grown to leverage the possibilities offered in terms of fabrication of visibly transparent prints and quick post-processing notwithstanding the slightly higher printer and running costs compared with FDM [31].

In the present study, we have prototyped a 3D-printed permeation unit, furnished with a semipermeable membrane support, and coupled to a sequential injection automatic analyzer that allows for the first-time continuous monitoring in both donor and acceptor compartments. Using the fluorescent tracer Rho123 that is transported by P-gly transporter of MDCKII-MDR1 cells in the presence of inhibitors, the novel 3D device is expected to improve the classical protocol of Rho123 permeation monitoring and the inhibition of P-gly-mediated transport, which lasts 8 h [3]. Following the basic design of a Franz-cell but decreasing the acceptor compartment volume, the research in this work complies with the guidelines for permeation testing but is expected to improve sensitivity, decrease laborious experimentation and enable

compensation of errors of tracer detection in the acceptor compartment. Additionally, monitoring of the tracer level in both compartments allows evaluating the amount of tracer accumulated inside cells. The developed 3D printed module has also been filed as a patent application [32].

2. Experimental

2.1. Chemicals and sample preparation

All chemicals were of analytical grade quality. Rhodamine 123 (Rho123), verapamil hydrochloride (Ver), and dimethyl sulfoxide (DMSO) were purchased from Sigma-Aldrich/Merck KGaA (Prague, Czech Republic). Cultivation medium (Opti-MEM reduced serum medium) for cell cultivation and for permeation testing was obtained from Gibco-ThermoFisher Scientific (Prague, Czech Republic).

A 200 μmol L^{-1} Rho123 stock solution was prepared by dissolving the appropriate amount in a small volume of DMSO and filled up with water. The final concentration of DMSO in working solutions did not exceed 0.1%. A 100 μmol L^{-1} Ver stock solution was prepared in water and then diluted with cultivation medium to the final concentration. Working solutions were prepared daily by dilution with water or cultivation medium. All solutions were kept at 4°C and protected against light.

Madin-Darby canine kidney type II live cells (MDCKII) stably transfected with human MDR1 (ABCB1) gene encoding P-glycoprotein (P-gp) under viral promoter control (MDCKII-MDR1) were used for pharmacokinetic experiments. The cell line has been kindly provided by Dr. Alfred Schinkel (The Netherlands Cancer Institute, Amsterdam) and cultivated in the Department of Pharmacology and Toxicology, Faculty of Pharmacy in Hradec Králové, in standard High-glucose DMEM medium supplemented with 10% Fetal Bovine Serum. Cultivation on polycarbonate inserts (24 mm Transwell® with polycarbonate membranes of 3.0 μm pore size, growth surface area 4.67 cm^2, Baria, Prague, Czech Republic) was done over three days to obtain an intact cell monolayer, prepared for permeation testing. Cells were seeded at the density of 100,000 cells per cm^2 on Transwell® dish and media were changed every day [33].

2.2. 3D printed permeation module

In this work, a new permeation module was 3D printed using stereolithographic technology (SLA). For the design, 123D design CAD software was used and printed objects

were obtained by a Form2 printer (Formlabs, Somerville, MA, USA) with a layer height of 50 µm (TriLAB Group s.r.o., Hradec Kralove, Czech Republic). The material used was Clear Resin (Formlabs) being a combination of polyacrylates according to the producer's description. Post-print processing consisted of removing the excess of resin with isopropanol, overnight curing under UV light at < 350 nm, and rework threat ports for flow-through analysis.

The design of the 3D printed module is depicted in Fig. 2 and Fig. 3. In short, it consisted of a modified Franz-cell chamber with sampling ports in the acceptor compartment, a lid that inhibited evaporation or contamination of the medium and enabled continuous sampling of the donor compartment as well, and a holder to secure the position of the device in a water bath or incubator. Several considerations on the cell design are discussed in section 3.1.

2.3. Sequential Injection System

The apparatus used for the automation of permeation tests was based on a Sequential Injection Analyzer (MicroSIA system, FIAlab® instruments, USA). The miniaturized flow manifold consisted of a 5 mL piston pump and a 6-port selection valve connected each other by a holding coil (HC, 400 µL volume). HC and further flow conduits were made from Fluorinated Ethylene Propylene (FEP) 1520 XL tubing of 0.75 mm i.d. An incubator Galaxy 14S (New Brunswick™, Eppendorf AG, Germany) was used to keep the permeation unit at a temperature of 37°C throughout. Continuous mixing of the content of the acceptor compartment of the 3D printed module was accomplished by an electromagnetic stirrer that was placed inside the incubator and using a miniature stirring bar (7 × 2 mm).

An additional Minipuls 3 peristaltic pump (Gilson®, USA) was used for continuous circulation of the cultivation medium (acceptor compartment) and the testing solution including cultivation medium, Rho123 and potentially Ver (donor compartment) via circulation loops as shown in Fig. 2. This enabled on-line sampling of representative fractions for determination of the contents of Rho123 and Ver in both compartments (in our study only Rho123 was determined). Each sampling loop consisted of a 150 cm long PTFE tubing integrating a 40 cm long peristaltic Tygon® pumping tube (1.02 mm i.d., Gilson®, USA) and a T-connector (Tee Assembly Tefzel®, 0.50 mm i.d. of the inner hole, Upchurch, Germany), which was used for low-dead volume sampling by connection to one of the selection valve lateral ports that communicated with the syringe pump. The peristaltic pump operated at 1.3 mL min^{-1}. A magnified view of the components of the 3D printed permeation module is shown in Fig. 3. Additionally, a close-up of the flow system is available in the Supplementary material.

A spectrofluorometer RF 6000 (Shimadzu Europa GmbH, Duisburg, Germany) equipped with a 120 µL quartz flow cell was used for detection of Rho123 only, with excitation at 475 nm (1.5 nm bandwidth), emission at 533 nm (3.0 nm bandwidth), an accumulation time of 50 ms, a cycle time of 0.20 s, and scanning frequency of 5 Hz. The Ver signal did not interfere with Rho123 fluorescence detection as proved experimentally. The flow system was controlled by the FIAlab® software for Windows 5.0 (FIAlab® instruments, USA). The spectrofluorometer was controlled by LabSolutions RF in Time Course mode (Shimadzu) for data acquisition and evaluation.

2.4. Analytical procedure

All solutions, including test solutions of Rho123 and Ver and cultivation medium, were placed inside the incubator set to a temperature of 37°C. Thermostability was reached within 20 min. Prior to start, the syringe pump and the detection line were filled with the carrier (Opti-MEM cultivation medium) and one port of the selection valve was washed with the cultivation medium that will be used to refill the volume of both compartments after sample aspiration during the permeation test. The acceptor compartment was then filled with 9 mL of cultivation medium and circulation was started by activation of the peristaltic pump and the magnetic stirrer. The permeation unit was placed inside the incubator for about 5 min to release air bubbles from degasification of the medium. Then, an insert with verified cell monolayer was taken from the incubator, leftovers of old cultivation medium were carefully pipetted off, and the insert was placed onto the permeation unit. Simultaneously, the test solution was pipetted into the donor compartment to avoid cell damage and monolayer delamination. This way, the donor compartment was filled with 4 mL of either Rho123 or combined Rho123-Ver solution, depending on the aimed permeation test. Monitoring was then started by initialization of the flow measurement procedure.

Automated monitoring was based on the following steps. At first, carrier was aspirated into the syringe pump. Then 100 µL of sample were aspirated from the respective sampling port (either acceptor or donor phase) for washing and avoiding sample carry-over and discarded to waste. Next, 50 µL of sample from the sampling port and respective circulation loop were aspirated into the holding coil and sent to the detection flow cell under the optimized flow rate of 30 µL s^{-1} by flow reversal. The sampling at each time interval was carried out twice as a compromise between improvement of measurement precision, prolongation of the analytical procedure, and sample consumption within the respective sampling period. With the carrier

passing through the detection flow cell after the sample segment, the system was cleaned and was ready for the next sampling. The measurement cycle was finished by compensating for the sampled volume, i.e. by dispensing an equal volume (namely, 200 µL) through the circulation loop into the respective compartment. The idea behind is to keep the total volume constant throughout the test and assure a steady contact of the liquid contained in the acceptor compartment with the cell monolayer. Dilution was further considered in the data evaluation step according to equation 1 (see below).

This procedure enabled taking samples automatically from both compartments in a user-defined frequency and obtaining a Rho123 concentration profile of high time resolution over the entire permeation test. Here the test lasted 2 h, which is much shorter time than the common monitoring time in off-line permeation testing (which might last up to 8 h). Based on our previous experience with real-time monitoring of such permeation test, we decided to set 2 h testing to investigate effects over the first interval of commonly longer permeation studies. Even in routine studies samples can be taken after 30 min, in 1 h, 2 h and in further periods. Our first testing [11] was carried out in 2 and 4 h format and 2 h were found enough to observe interactions of substrates and inhibitors with P-gly. Selection of volumes and flow rates of the respective procedural steps was carried out together with setting the intervals and sequence of sampling from the donor and acceptor compartments (see below).

2.5. Selection of parameters and data evaluation

Experimental variables were investigated with respect to the detectability of Rho123 in the acceptor compartment because just several percent of the original concentration applied to donor compartment were expected to pass into the acceptor compartment. External calibration graphs for Rho123 determination obtained with aqueous solutions and solutions prepared with cultivation medium, used during permeation testing, were compared. In this step, different sample volumes and flow rates for detection, including 50 and 60 µL at 20 and 30 µL s^{-1}, respectively, were tested. The sensitivity was compared with analysis time to get quick but precise Rho123 determination. The linearity of response was tested in the range of 2.5 to 50 µmol L^{-1} Rho123.

Evaluation of data obtained in the permeation tests was based on the recalculation of the Rho123 concentration in the respective sampling time using external calibration on the same day. This recalculation was needed to compensate for the dilution of the compartment contents with fresh cultivation medium after each sampling. Recalculation, following our previous work [12], was done according to equation 1 for which C_n is the concentration of *n*-sample:

$$C_{n,\text{corrected}} = C_{n,\text{measured}} + (\text{Volume}_{(\text{sample})}/\text{Volume}_{(\text{acceptor or donor})}) \times C_{n-1,\text{measured}} \quad (1)$$

3. Results and discussion

3.1. Design of the 3D printed permeation module

Our previous study based on the application of a glass Franz cell to monitor drug permeation demonstrated the possibility of monitoring the Rho123 concentration profile in the acceptor compartment in real-time [11]. However, the previous design was merely able to monitor the acceptor compartment, was suitable only for small inserts for which monolayers might contain an insufficient number of cells, and suffered from high dilution of the analyte Rho123 that was transported from a small donor to a large acceptor compartment.

To tackle the above limitations, we herein propose an improved design capitalized on SLA 3D printing aimed at increasing the donor compartment diameter so that wider inserts with considerably larger membrane area could be used. Moreover, the shape of the permeation unit is modified (concave shape) to decrease the volume of the acceptor compartment to avoid unnecessarily high analyte dilution that jeopardized detectability of the marker, yet allowing the use of a magnetic stirring bar to ensure fast homogenization of the acceptor compartment content. The upper part was also modified by adding a convex covering lid that reduces evaporation and avoids the accumulation of condensate that would drop into the donor compartment and disturb the cell monolayer integrity. Also, a holder allowed simple click-fixation of the permeation device.

Moreover, sampling inlets and outlets were implemented in the 3D model to accomplish for the first-time sampling from circulating medium in both compartments with possible adjustment of the penetration depth of the connecting tubing. This way, easy estimation of the fluorescent marker content inside cells is feasible in real-time without the need of cell lysis. Finally, wall thickness of the permeation device was reduced as much as possible to improve heat transfer, which is, given the polymer material, worse than in glass permeation devices. The consumption of material for the permeation device and lit is less than 2 × 10 mL resin corresponding to a fabrication cost of less than 4 € with a few hours printing time only.

In Table 1, the main differences towards the commercial cells are summarized: (i) the used material but most importantly (ii) the four times larger permeation area, i.e., the surface that can be covered by a cultivated monocellular layer, and (iii) the reduced acceptor compartment volume by about factor 2. In consequence, a significant improvement in the ratio of the permeation area to the acceptor volume was achieved (about eight times higher for the

3D printed cell); thus the detection sensitivity, i.e., traceability of the target components that will permeate through the cellular monolayer is equally improved. This also allows study permeation processes with lower, more realistic concentrations of the analytes of interest.

On the other hand, the ratios of the volume to the inner surface of the acceptor compartment are comparable for both kinds of cells because the same level of liquid in the donor compartment is used in all instances. The heat transfer is admittedly worse through plastics than through glass, and thus, the wall thickness of the 3D printed module is about 25% thinner compared to the glass counterparts.

Moreover, commercial Franz cells feature, in some cases, heat-sleeves for a direct connection to a thermostated water bath. However, considering that a constant temperature can also be obtained with a thermostated oven (as it was done in this work) and the fact that in such a case flexible tubing connection to the permeation module is not required, and that the possibility to generate an altered atmospheric composition (e.g., enhanced CO_2 level) is now easily accomplished, we consider the use of heat-sleeves of marginal relevance in the practical use of the cells.

3.2. Analytical performance of the automated monitoring procedure

The calibration in aqueous solutions prepared off-line was linear in the range of 5 to 40 μmol L^{-1} of Rho 123 with a determination coefficient of 0.9930. The calibration in cultivation medium using a sample volume of 60 μL and a flow rate of 20 μL s^{-1} for detection revealed linearity from 5 to 50 μmol L^{-1} (R^2 = 0.9968); with 50 μL and 30 μL s^{-1} in the range of 2.5 to 50 μmol L^{-1} (R^2 = 0.9964), that is better than in aqueous standards. Thus, the last combination was applied to permeation testing to yield a wider linear range and a shorter time of analysis. Limits of quantitation (LOQ) and detection (LOD) were calculated based on the signal corresponding to 10 and 3-times the baseline noise level, respectively. The LOQ was equal to the lowest concentration of the linear working range, i.e., 2.5 μmol L^{-1} and the LOD was 0.8 μmol L^{-1}.

Water does not affect permeation, but it might influence viability of cells due to osmolarity change and thus cultivation medium should be used throughout the whole permeation test. One measurement cycle took 4 min followed by 1 min delay to accomplish 5 min sampling intervals. Sampling from the donor compartment and acceptor compartment were alternated. This way, concentration profiles with sample intervals of 10 min were obtained with sampling started at 0 min for the donor and at 5 min for the acceptor compartment. The overall

monitoring included 24 sampling points. Thus, 12 sampling points from the donor and 12 from the acceptor compartments served to describe the profiles of interaction in real-time of Rho123 alone as a substrate or in combination with Ver as an inhibitor of P-gly membrane transporter.

In case of changing tracer or just in between measurements the washing of the whole flow system including the 3D printed module with isopropanol or ethanol is highly recommended. Then, fresh cultivation medium tempered to 37°C should be used to fill the system before replacement of the testing solution.

3.3. Comparison of kinetic profiles obtained in permeation tests

In the beginning, the 3D printed material (SLA Clean Resin) was immersed into an aqueous 20 μmol L^{-1} Rho123 solution at different time periods including 1 h, 2 h, 3 h, 4 h, and 48 h for comparison (See Supporting Information). Then, the fluorescence signal of Rho123 solution was measured and close-ups of the prints were undertaken to investigate the potential adsorption of Rho123 onto the surface of the 3D printed material. With this experiment, the release of monomers from the tested 3D printed pieces affecting the fluorescence signal could be detected. A slight yet visible change of the prints attributed to the sorption of the marker was found after 1 h, but the differences between fluorescence signals in the 4 h experiment did not exceed 6 %. A similar experiment was carried out with pure cultivation medium and medium applied after immersion of the objects in Rho123 solution for 48 h and cleaning with methanol. The results illustrated in Supplementary material revealed that changes of the fluorescence signal were below 3% of the original fluorescence signal.

Preliminary assays were undertaken to explore the compatibility of the 3D printed material with living cells. First, a permeation experiment was carried out without cell monolayer to obtain a kinetic profile corresponding to passive diffusion as is the case with those tests with weak cell adherence to the support. The same behavior would be expected when leakage of monomers from the 3D material occurs as this would, in turn, affect cells' comfort and growth conditions. Passive diffusion was monitored for 100 and 50 μmol L^{-1} Rho123, while in each sampling point, a decrease of the marker in the donor compartment and an increase in the acceptor compartment was found with steady-state conditions being reached at 60 and 50 min, respectively. The results for 100 μmol L^{-1} Rho123 are documented in Supplementary material. Further, the kinetic profiles obtained in cell-based permeation testing were compared with those of the above profile of passive diffusion to assert any problem related to toxic substances in the circulated solutions that could originate from the 3D printed permeation module.

Automated permeation tests with cell monolayers were based on the on-line determination of Rho123 in both compartments. The original concentration of the marker in the donor compartment was varied from 10 μmol L^{-1} to 20 μmol L^{-1}. Rho123 was tested separately and in combination with Ver as P-gly inhibitor that will block membrane transporter and thus enable Rho123, as a substrate, to be transferred by passive diffusion across/inside the cell monolayer. Ver concentration was increased throughout this work from 20 μmol L^{-1} to 100 μmol L^{-1}. Several ratios of Rho123 against Ver were tested (viz., 2:5, 1:5, and 1:10) to differentiate the interaction of the inhibitor against Rho123. Ver is also a weak substrate of P-gly, there is competition for the transporting site (channel) inside the transporter. Thus, higher concentration of Ver (lower Rho123:Ver ratio) results in a more efficient inhibition of Rho123 transport. The marker:inhibitor ratio needed to visualize membrane transporter inhibition together with the time of competitive interaction with P-gly need to be explored in every application to get insight into the inhibition effect of Ver.

In the first set of experiments, we used 20 μmol L^{-1} of Rho123 and 50 μmol L^{-1} of P-gly inhibitor Ver in the donor compartment. In case of a permeation study with Rho123 alone, we observed a decrease in the concentration of biomarker in the donor compartment (mainly because of paracellular transport) with a decrease rate of 0.6 Rho123 μg h^{-1} and an increase in the acceptor compartment with the same rate 0.6 μg h^{-1}. Both rates were calculated using data obtained in the period of 50-110 min in the donor compartment and 55-115 min in acceptor compartment. When Ver was added, Rho123 disappeared in the donor compartment much faster with a rate 1.0 μg h^{-1} and appeared in the acceptor compartment with a rate 0.8 μg h^{-1}. Importantly, the permeation was observed much easily in the novel 3D printed module in comparison with traditional insert permeation experiments for which the first data point is usually measured after 30 min or 1 h. We analyzed Rho123 in the acceptor side from the 5th minute. This is due to the fast mixing of the medium with biomarker and Ver at the donor side in our recirculation-based flow system. In the presence of Ver, the ratio of Rho123 concentration in donor versus acceptor tends to 1 for the whole experiment, thus indicating a fast and free transport of Rho123 across the cellular monolayer without the effect of reversal pumping by P-gly at the apical membrane. We suppose that the permeation is here via both transcellular and paracellular transport mechanisms (Fig. 4). In all experiments, an initial decrease of the original Rho123 concentration in the donor compartment is observed by the dilution of the tested solution in the overall volume of the donor compartment, which includes pure cultivation medium from the circulation loop.

In the next experiment, we decreased the concentration of Rho123 in the donor compartment to 10 μmol L^{-1}. We observed a gradual decrease in Rho123 concentration in the donor compartment with a rate 0.2 μg h^{-1} and a gradual increase of concentration in the acceptor compartment with a similar rate as it was the case with 20 μmol L^{-1} described above. Interestingly, when we added P-gly inhibitor Ver into the donor compartment, we observed a lower concentration of Rho123 in the donor compartment (faster disappearance rate: 1.0 μg h^{-1}) as expected, but a lower concentration in the acceptor compartment (rate of 0.5 μg h^{-1}) in comparison with the experiment performed without Ver (Fig. 5). As before, the same dilution in the donor sampling loop was observed..

In another experiment, we performed permeation studies with 100 μmol L^{-1} Ver while keeping Rho123 at 10 μmol L^{-1}. We observed an almost similar pattern of Rho123 penetration as in Fig. 5. 100 μmol L^{-1} Ver facilitated Rho123 transport into the cells with a rate of 0.7 μg h^{-1} but again lower concentration (compared to Rho123 alone) of the marker was found in the acceptor with a transfer rate of 0.4 μg h^{-1}. Ratios of donor versus acceptor for Rho123 concentration in both experiments (with and without inhibitor) with time showed a virtually identical decreasing trend regardless of the presence of Ver in the media. The unexpectedly low concentration of Rho123 in the acceptor is attributed to the accumulation of the marker in the cell monolayer during the assays. The difference in the behavior of red lines in the right part of Fig. 5 can be explained by a more efficient inhibition of P-gly while incresing Ver concentration.

Fig. 6 shows that Ver systematically increases the amount of Rho123 accumulated in cells from the donor compartment for incubation periods ≥ 100 min. Therefore, we suppose that Rho123 at the concentration of 10 μmol L^{-1} enters easily into cells when P-gly is efficiently inhibited by high concentrations of Ver, but due to the low donor concentration of marker, it preferentially accumulates in cells (Fig. 6) and do not penetrate into the acceptor compartment as in the case of 20 μmol L^{-1}. Thus, we can conclude that the use of low concentrations of Rho123 in the experimental set-up (≤ 10 μmol L^{-1}) serves to investigate only the entry into the cell monolayer but not the permeation itself. Importantly, both set-ups with either low or high concentration of Rho123 reliably and quickly inform us if a tested compound inhibits P-gly. However, the monitoring of the ratios between donor and acceptor for Rho123 might be misleading for low marker concentrations. Instead, the continuous on-line determination of the marker concentrations in both compartments at high temporal resolution as obtained by flow systems is mandatory for elucidation of inhibition effects.

Additionally, when the effects of Ver at concentrations of 50 and 100 μmol L^{-1} were compared, a slight decrease of the rate of Rho123 into the donor compartment was observed in case of 100 μmol L^{-1}. This might be explained due to the non-specific inhibition of Ver in the kidney cell line, in which many other transporters display some residual expression [35]. No further increase of the rate also suggests that the concentration of 50 μmol L^{-1} saturates the P-gly and leads to complete inhibition of P-gly in our model, which correlates with the inhibition constant of Ver for P-gly (IC_{50} = 2.1 μmol L^{-1}) [35].

Evaluation of accumulated Rho123 in cells can be affected by sticking of the marker to the outer cellular membrane and keep adhered in the lysate. Thus cell lysis may not help determine Rho123 inside cells. For P-gly substrates that are lipophilic or stick to outer membrane, an indirect method considering both donor and acceptor concentrations is more suitable to determine intracellular accumulation. In the following papers [36-42], authors describe accumulation of Rho123 in MDCKII-MDR1 cells after treatment with Ver or other P-gly inhibitors in MDCKII-MDR1 cells. It is difficult to compare their data with our predictions, but we might assume that these inhibitors usually double intracellular concentration of Rho123 in MDCKII-MDR1 cells. This agree with our results in Fig. 6.

4. Conclusion

Automated monitoring of cell permeation studies using the proposed 3D printed permeation module based on the modified Franz cell design benefited from the possibility of on-line sampling from both donor and acceptor compartments. Thereby, full insight into the cell permeation of Rho123 as a fluorescent marker was possible including the assessment of Rho123 concentration inside the cells in real-time by evaluation of the difference between concentrations in both compartments without user's intervention. Washing, continuous sampling, on-line determination of the fluorescent marker and solution replenishment of both compartments were fully automated.

The developed 3D printed permeation unit differs from the original Franz cell design in (i) the volume of the acceptor compartment, (ii) possibility of sampling from both compartments, (iii) use of a cover in the donor compartment, and (iv) fit-for-purpose fabrication from a photo-polymerizable SLA resin. Adaptation of both compartments´ volumes enabled utilization of (i) larger surface of cell monolayers in wide inserts, (ii) lower concentration levels of the tracer (higher sensitivity is obtained by the decrease of acceptor volume), (iii) monitoring of concentration inside cells in real-time without the need of cell lysis, and (iv) experimental

conditions that better mimic the interaction of exogenic compounds with cells and their membrane transporter systems. The kinetic profiles obtained in our tests corresponded to concentration changes in real-time. In consequence, transporter inhibition could be evaluated either by monitoring the tracer concentration in both compartments (ratios similar to 1 during the time-course experiment indicate inhibition) or by the time of competitive interaction of substrate and inhibitor, the shorter the time to observe a donor to acceptor ratio of 1 for the substrate the larger is the inhibitory effect.

Franz cells are usually made of glass because this material is inert with respect to adherence of the tested substances. The risk of potential adsorption of substrates and inhibitors to the surface of all used materials should always be tested. In our case, post-print processing was sufficient to close the pores on the surface of the printed object and thus, no significant adsorption was observed in 2 h measurements. Also, the risk of monomer leakage from the photopolymerized device should be taken into account because monomers can affect the growth conditions of living cells. We have not found any cell monolayer damage that will cause passive diffusion in such permeation testing. However, there are now biocompatible 3D printing resins available and their long-time stability, in particular, in regards of monomer leakage, adsorption characteristics for permeation tracers such as Rho123, and their compatibility with living cells should be investigated.

In addition, fabrication of identical permeation units by 3D printing is possible in any remote laboratory by transfer of .stl-files so that the same design or prototype can be used for permeation testing by other scientists, thus increasing inter-laboratory comparability.

Acknowledgement

This work was supported by the EFSA-CDN project (Reg. No. CZ.02.1.01/0.0/0.0/16_019/0000841) co-funded by ERDF and by the Project of Specific Research, SVV No. 260 548. The authors also acknowledge financial support from the FEDER/Spanish Ministry of Science, and Innovation (MICINN)-Spanish State Research Agency (AEI) through project CTM2017-84763-C3-3-R. This article is based upon work from the Sample Preparation Task Force and Network, supported by the Division of Analytical Chemistry of the European Chemical Society.

Literature

[1] D.A. Volpe, Drug-permeability and transporter assays in Caco-2 and MDCK cell lines, Future Med. Chem. 3(16) (2011) 2063-77.

[2] M. Alberti, Y. Dancik, G. Sriram, B. Wu, Y.L. Teo, Z. Feng, M. Bigliardi-Qi, R.G. Wu, Z.P. Wang, P.L. Bigliardi, Multi-chamber microfluidic platform for high-precision skin permeation testing, Lab Chip 17 (2017) 1625-1634.

[3] J.B. da Silva Junior, T.M. Dezani, A.B. Dezani, C.H. dos Reis Serra, Evaluating potential P-gp substrates: main aspects to choose the adequate permeability model for assessing gastrointestinal drug absorption, Mini Rev. Med. Chem. 15(10) (2015) 858-71.

[4] H.E. Abaci, K. Gledhill, Z. Guo, A.M. Christiano, M.L. Shuler, Pumpless microfluidic platform for drug testing on human skin equivalents, Lab Chip 15 (2015) 882-888.

[5] F. Sivandzade, L. Cucullo, In-vitro blood-brain barrier modeling: A review of modern and fast-advancing technologies, J. Cereb. Blood Flow Metab. 38 (2018) 1667-1681.

[6] M.J. Zamek-Gliszczynski, M.E. Taub, P.P. Chothe, X. Chu, K.M. Giacomini, R.B. Kim, A.S. Ray, S.L. Stocker, J.D. Unadkat, M.B. Wittwer, C. Xia, S.W. Yee, L. Zhang, Y. Zhang, International transporter consortium. Transporters in drug development: 2018 ITC recommendations for transporters of emerging clinical importance, Clin. Pharmacol. Ther. 104(5) (2018) 890-899.

[7] EMA guideline 2012. Guideline on the investigation of drug interactions. CPMP/EWP/560/95/Rev. 1 Corr. 2** Committee for Human Medicinal Products (CHMP). 21 June 2012.

[8] FDA Guidance for Industry 2020. In vitro drug interaction studies - Cytochrome P450 enzyme- and transporter-mediated drug interactions. Chapter IV. Evaluating Transporter-Mediated Drug Interactions Guidance for Industry. Food and Drug Administration. January 2020.

[9] I. Cascorbi, P-glycoprotein: tissue distribution, substrates, and functional consequences of genetic variations, Handb. Exp. Pharmacol. 201 (2011) 261-83.

[10] H. Glaeser, Importance of P-glycoprotein for drug-drug interactions. Handb. Exp. Pharmacol. 201 (2011) 285-97.

[11] L. Zelená, S. Marques, M. Segundo, M. Miró, P. Pávek, H. Sklenářová, P. Solich, Fully automatic flow-based device for monitoring of drug permeation across a cell monolayer, Anal. Bioanal. Chem. 408 (2016) 971-981.

[12] J. Klimundová, K. Mervartová, H. Sklenářová, P. Solich, M. Polášek, Automated sequential injection fluorimetric set-up for multiple release testing of topical formulation, Anal. Chim. Acta 573–574 (2006) 366–370.

[13] J. Klimundová, D. Šatínský, H. Sklenářová, P. Solich, Automation of simultaneous release tests of two substances by sequential injection chromatography coupled with Franz cell, Talanta 69 (2006) 730-735.

[14] P.D. Tzanavaras, A. Verdoukas, T. Balloma, Optimization and validation of a dissolution test for famotidine tablets using flow injection analysis, J. Pharm. Biomed. Anal. 41 (2006) 437-441.

[15] A.M. Pimenta, M.C.B.S.M. Montenegro, A.N. Araujo, J. Martínez-Calatayud, Application of sequential injection analysis to pharmaceutical analysis, J. Pharm. Biomed. Anal. 40 (2006) 16-34.

[16] S.A. Motz, J. Klimundova, U.F. Schaefer, S. Balbach, T. Eichinger, P. Solich, C.M. Lehr, Automated measurement of permeation and dissolution of propranolol HCl tablets using sequential injection analysis, Anal. Chim. Acta 581 (2007) 174–180.

[17] A.C. Alves, I. Ramos, C. Nunes, L.M. Magalhaes, H. Sklenářová, M. Segundo, J.L.F.C. Lima, S. Reis, On-line automated evaluation of lipid nanoparticles transdermal permeation using Franz diffusion cell and low-pressure chromatography, Talanta 146 (2016) 369-374.

[18] Permegear, https://permegear.com/in-line-cells/ (accessed June 5, 2020)

[19] M.J.C. Santbergen, M. van der Zande, A. Gerssen, H. Bouwmeester, M.W.F. Nielen, Dynamic in vitro intestinal barrier model coupled to chip-based liquid chromatography mass spectrometry for oral bioavailability studies, Anal. Bioanal. Chem. 412 (2020) 1111-1122.

[20] X. Guo, Q. Cao, Y. Liu, T. He, J. Liu, S. Huang, H. Tang, M. Ma, Organic electrochemical transistor for in situ detection of H_2O_2 released from adherent cells and its application in evaluating the in vitro cytotoxicity of nanomaterial, Anal. Chem. 92 (2020) 908-915.

[21] P.N. Nesterenko, 3D printing in analytical chemistry: current state and future, Pure Appl. Chem. 92 (2020) 1341–1355.

[22] A.K. Au, W. Huynh, L.F. Horowitz, A. Folch, 3D-Printed Microfluidics, Angew. Chem. Int. Ed. 55 (2016) 3862-3881.

[23] B. Gross, S.Y. Lockwood, D.M. Spence, Recent Advances in Analytical Chemistry by 3D Printing, Anal. Chem., 89 (2017) 57.

[24] D.J. Cocovi-Solberg, P.J. Worsfold, M. Miró, Opportunities for 3D printed millifluidic platforms incorporating on-line sample handling and separation, Trends Anal. Chem. 108 (2018) 13-22.

[25] F. Li, M. Rodas Ceballos, S. Keshan Balavandy, J. Fan, M. Mahdi Khataei, Y. Yamini, F. Maya, 3D Printing in analytical sample preparation, J. Sep. Sci. 43 (2020) 1854-1866.

[26] U. Kalsoom, P.N. Nesterenko, B. Paull, Current and future impact of 3D printing on the separation sciences, Trends Anal. Chem. 105 (2018), 492-502.

[27] E.J. Carrasco-Correa, D.J. Cocovi-Solberg, J.M. Herrero-Martínez, E.F. Simó-Alfonso, M. Miró, 3D printed fluidic platform with in-situ covalently immobilized polymer monolithic column for automatic solid-phase extraction, Anal. Chim. Acta 1111 (2020) 40-48.

[28] D.J. Cocovi-Solberg, M. Rosende, M. Michalec, M. Miró, 3D Printing: The second dawn of Lab-On-Valve fluidic platforms for automatic (bio) chemical assays, Anal. Chem. 91 (2019) 1140-1149.

[29] C. Chen, Y. Wang, S.Y. Lockwood, D.M. Spence, 3D-printed fluidic devices enable quantitative evaluation of blood components in modified storage solutions for use in transfusion medicine, Analyst 139 (2014) 3219-226.

[30] K.B. Anderson, S.Y. Lockwood, R.S. Martin, D.M. Spence, A 3D printed fluidic device that enables integrated features, Anal. Chem. 85 (2013) 5622-5626.

[31] G.I. Salentijn, P.E. Oomen, M. Grajewski, E. Verpoorte, Fused Deposition Modeling 3D Printing for (Bio)analytical Device Fabrication: Procedures, Materials, and Applications, Anal. Chem. 89 (2017) 7053-7061.

[32] H. Sklenářová, P. Pávek. B. Horstkotte, P. Solich, M. Miró, Module for on-line monitoring of permeation tests, Czech patent application 2020-152.

[33] P. Pavek, G. Merino, E. Wagenaar, E. Bolscher, M. Novotna, J.W. Jonker, A.H. Shinkel, Human breast cancer resistance protein: Interactions with steroid drugs, hormones, the dietary carcinogen 2-amino-1-methyl-6-phenylimidazo(4,5-b)pyridine, and transport of cimetidine. J. Pharmacol. Exp. Ther. 312(1) (2005) 144-152.

[34] J. Klimundová, H. Sklenářová, U.F. Schaefer, P. Solich, Automated system for release studies of salicylic acid based on a SIA method, J. Pharm. Biomed. Anal. 37 (2005) 893-898.

[35] J. König, F. Müller, M.F. Fromm, Transporters and drug-drug interactions: important determinants of drug disposition and effects, Pharmacol. Rev. 65(3) (2013) 944-66.

[36] H. Jin, Y. Zhu, C. Wang, Q. Meng, J. Wu, P. Sun, X. Ma, H. Sun, X. Huo, K. Liu, A. Tan, Molecular pharmacokinetic mechanism of the drug-drug interaction between genistein and repaglinide mediated by P-gp, Biomed. Pharmacother. 125 (2020) 110032.

[37] W. Dong, Z.G. Liao, G.W. Zhao, X.J. Guan, J. Zhang, X.L. Liang, M. Yang, Reversal Effect of Oxypeucedanin on P-glycoprotein-mediated Drug Transport, Molecules 23 (2018) 1841.

[38] A. Ferreira, A.O. Santos, A. Falcão, G. Alves, In vitro screening of dual flavonoid combinations for reversing P-glycoprotein-mediated multidrug resistance: Focus on antiepileptic drugs, Food Chem. Toxicol. 111 (2018) 84-93.

[39] Z.G. Liao, T. Tang, X.J. Guan, W. Dong, J. Zhang, G.W. Zhao, M. Yang, X.L. Liang, Improvement of Transmembrane Transport Mechanism Study of Imperatorin on P-Glycoprotein-Mediated Drug Transport, Molecules 21 (2016) 1606.

[40] L. Pan, H. Hu, X. Wang, L. Yu, H. Jiang, J. Chen, Y. Lou, S. Zeng, Inhibitory Effects of Neochamaejasmin B on P-Glycoprotein in MDCK-hMDR1 Cells and Molecular Docking of NCB Binding in P-Glycoprotein, Molecules 20 (2015) 2931-2948.

[41] L. Yu, Q. Shen, Q. Zhou, H. Jiang, H. Bi, M. Huang, H. Zhou, S. Zeng, In vitro characterization of ABC transporters involved in the absorption and distribution of liensinine and its analogs, J. Ethnopharmacol. 150 (2013) 485–491.

[42] S. Ibrahim, J. Peggins, A. Knapton, T. Licht, A. Aszalos, Influence of beta-adrenergic antagonists, H1-receptor blockers, analgesics, diuretics, and quinolone antibiotics on the cellular accumulation of the anticancer drug, daunorubicin: P-glycoprotein modulation, Anticancer Res. 21 (2001) 847-856.

Table 1: Comparison of the 3D printed permeation module with commercial Franz cells

Characteristic	3D printed permeation module	Commercial Franz cell (values for 2 products) [11]
Material	acrylate/methacrylate resin	glass
Insert diameter (mm)	24	12
Area available for cell culture (cm^2)	4.67	1.12
Volume of acceptor compartment (mL)	7.8	15 / 14
Surface area of the acceptor compartment in contact with medium (cm^2)	1.68	3.64 / 3.18
Average wall thickness (mm)	ca. 1	1.25
Ratio of donor volume to cell culture surface (mL/cm^2)	4.64	4.12 / 4.40
Ratio of culture surface to acceptor volume (cm^2/mL)	0.6	0.075 / 0.080
Sampling from compartment	donor / acceptor	acceptor
Time interval (min)	10 / 10	- / 10
Sample repetitions	2	3
Volume (µL)	50	20
Length of the permeation test (h)	2	2-4
Rho123 concentrations tested (µmol L^{-1})	20,10	200,100

Figure captions

Fig. 1: Illustration of the setup for the permeation test using a commercial insert and representation of the P-glycoprotein function. P-glycoprotein transporter, localized in the apical (upper) membrane, actively pumps their substrates from cells into the donor compartment. In this manner, P-glycoprotein obstructs permeation from the donor compartment into acceptor compartment. P-glycoprotein inhibitors, thus, accelerate the permeation in the donor-to-acceptor compartment direction.

Fig. 2: Sequential injection system for on-line monitoring of permeation tests in real time A close-up of the flow system is available in the Supplementary material.

Fig. 3: 3D printed permeation unit design; A – insert with the tested cell monolayer as donor compartment; B – body of the permeation module; C – permeation unit lid with inlet and outlet from the donor compartment; D – support of the permeation unit to be placed in water bath or incubator. The heating medium (water or air) can flow through the openings so that the support does not exhibit any hindrance to heat transfer; E – inlet and outlet from the acceptor compartment; F – magnetic stirring bar.

Fig. 4: Interaction mechanism and comparison of kinetic profiles of Rho123 permeation using the MDCKII-MDR1cell line for 20 μmol L^{-1} Rho123 alone (black) and in combination with 50 μmol L^{-1} Ver at the ratio 2:5 (red). Inhibition of reverse pumping of Rho 123 via P-glycoprotein enables more intensive permeation of Rho 123 across the cellular monolayer. The P-glycoprotein inhibitor Ver thus accelerates transcellular transport and release into the acceptor compartment.

Fig. 5: Comparison of kinetic profiles of Rho123 permeation using the MDCKII-MDR1 cell line for 10 μmol L^{-1} Rho123 alone (black) and in combination with 50 and 100 μmol L^{-1} Ver at the ratio 1:5 and 1:10 (red).

Fig. 6: Temporal profiles of Rho123 accumulation inside MDCKII-MDR1 cells and comparison of accumulation of 10 μmol L^{-1} Rho123 in combination with 50 (red) and 100 (orange) μmol L^{-1} Ver against 10 μmol L^{-1} Rho123 alone (black). Inhibition of P-glycoprotein with the inhibitor Ver increases cellular accumulation of Rho 123 in MDCKII-MDR1 cells at 10 μmol L^{-1}. At this concentration of Rho 123, the tracer is mainly captured in cells at the end of the monitoring interval.

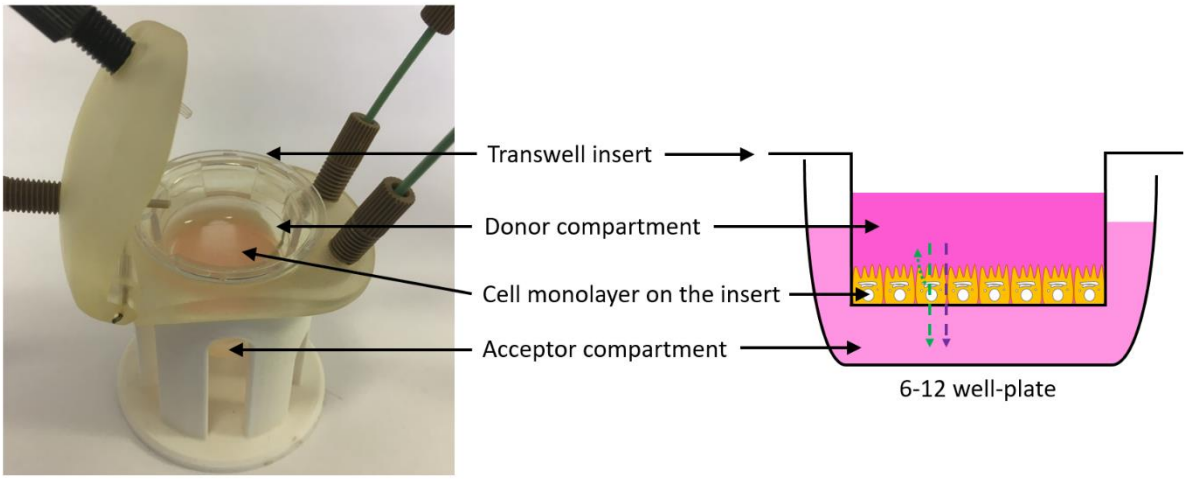
Transwell insert
Donor compartment
Cell monolayer on the insert
Acceptor compartment
6-12 well-plate

Figure 1

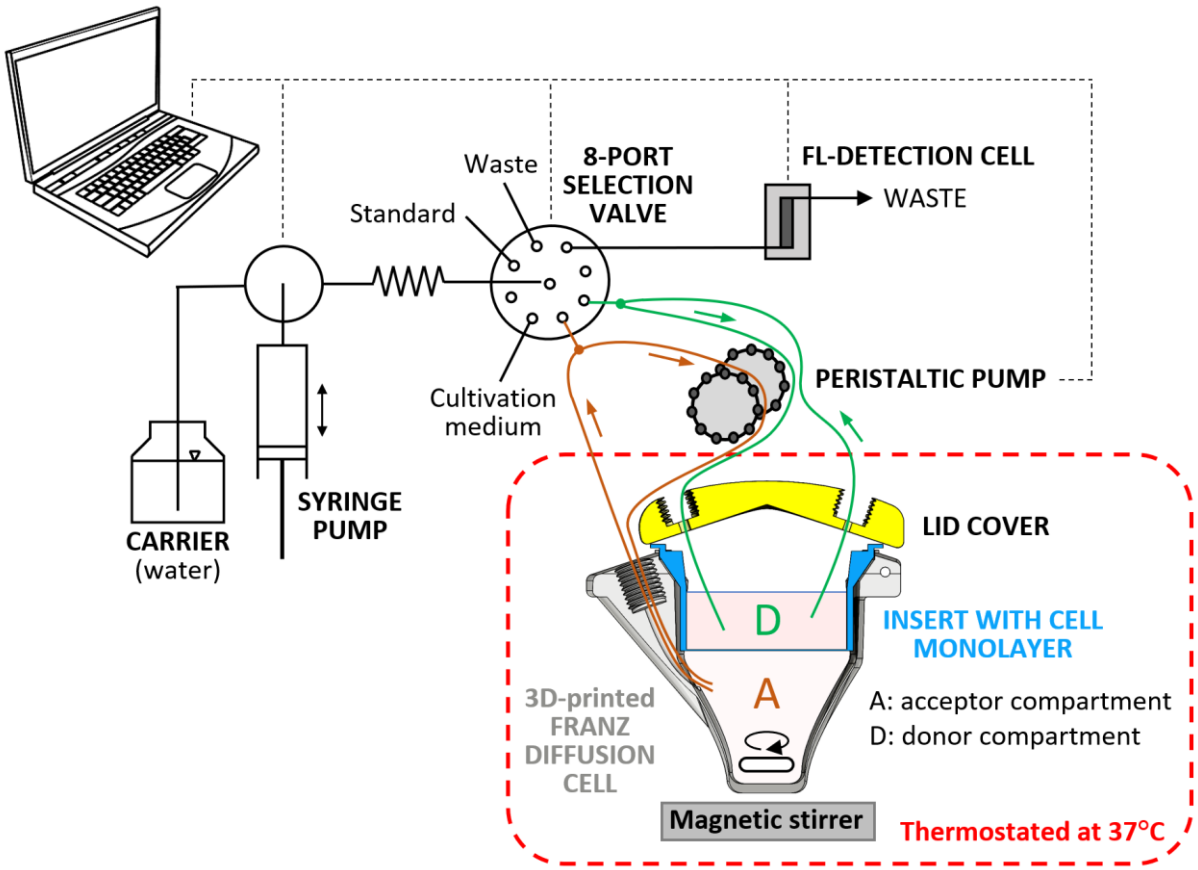
Waste
8-PORT
SELECTION
VALVE
FL-DETECTION CELL
Standard
WASTE
Cultivation
medium
PERISTALTIC PUMP
SYRINGE
PUMP
CARRIER
(water)
LID COVER
D
INSERT WITH CELL
MONOLAYER
A
3D-printed
FRANZ
DIFFUSION
CELL
A: acceptor compartment
D: donor compartment
Magnetic stirrer
Thermostated at 37°C

Figure 2

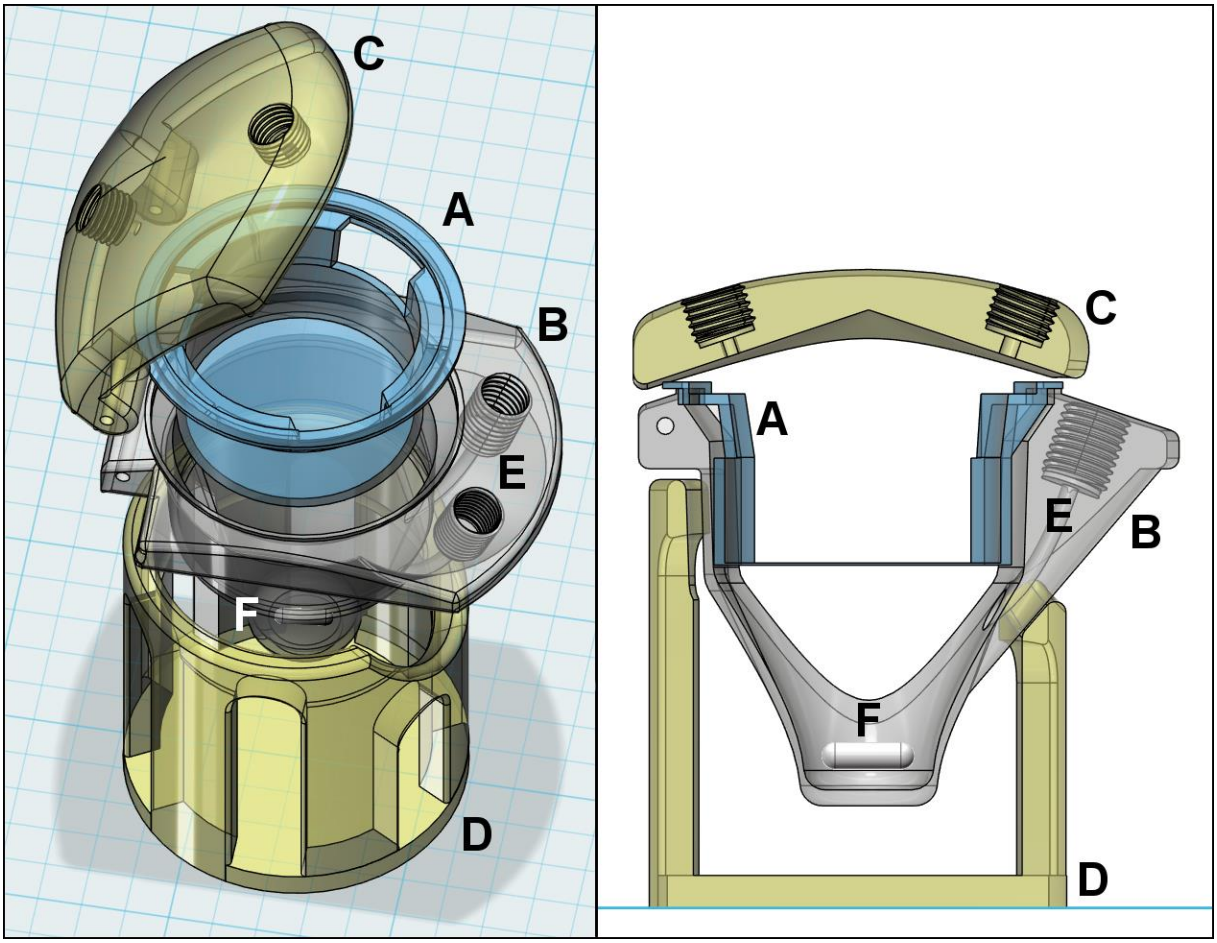

Figure 3

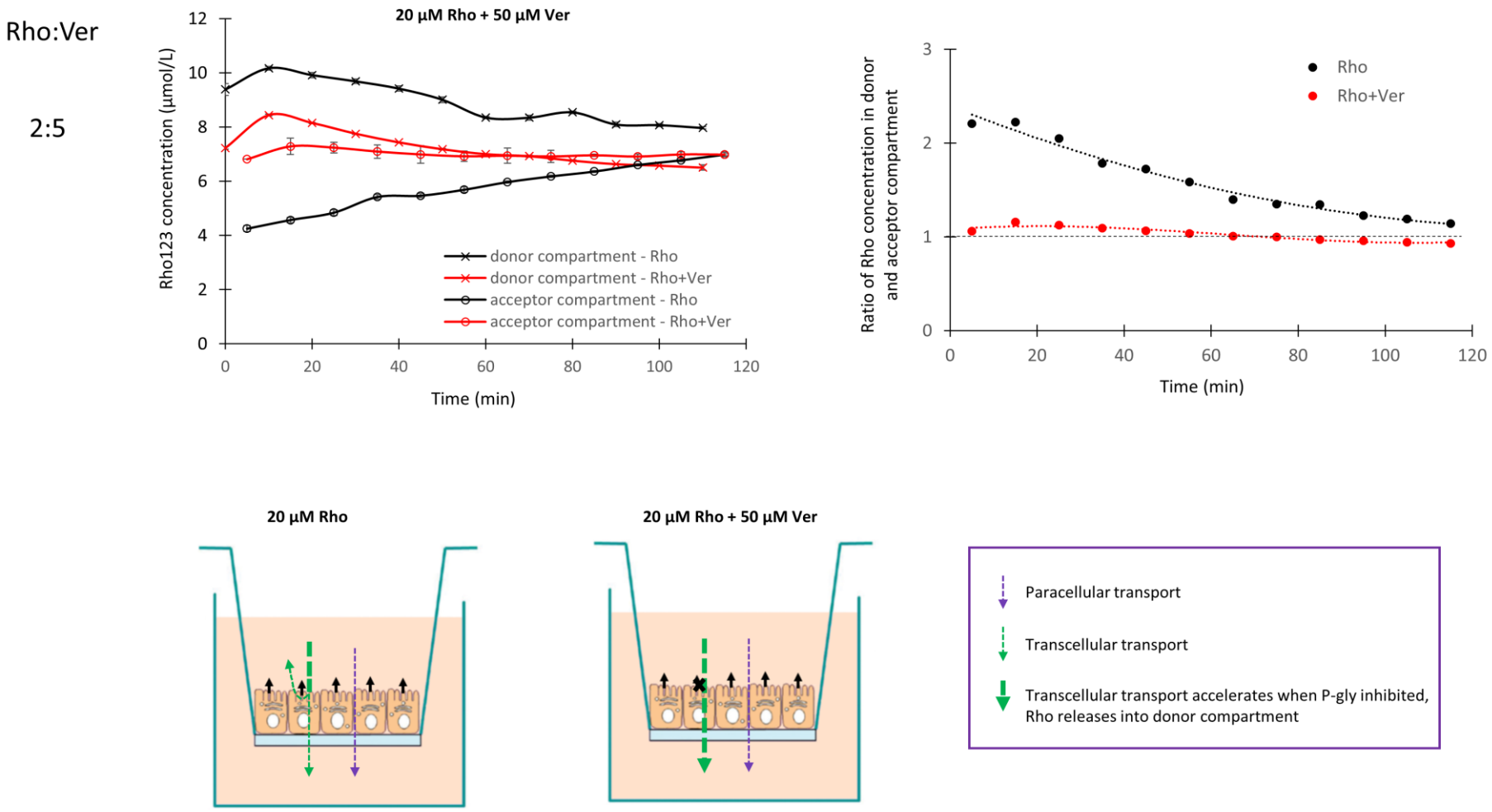
Rho:Ver
2:5
20 µM Rho + 50 µM Ver
Rho123 concentration (µmol/L)
Time (min)
donor compartment - Rho
donor compartment - Rho+Ver
acceptor compartment - Rho
acceptor compartment - Rho+Ver
Ratio of Rho concentration in donor and acceptor compartment
Rho
Rho+Ver
20 µM Rho
20 µM Rho + 50 µM Ver
Paracellular transport
Transcellular transport
Transcellular transport accelerates when P-gly inhibited, Rho releases into donor compartment

Figure 4

Rho:Ver

1:5

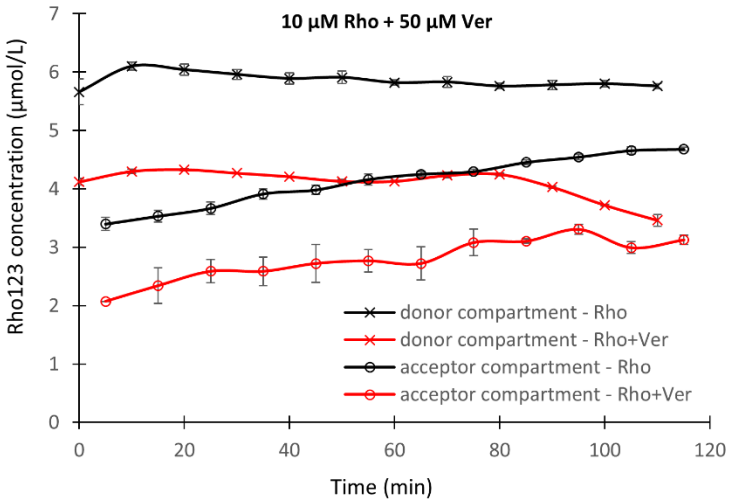

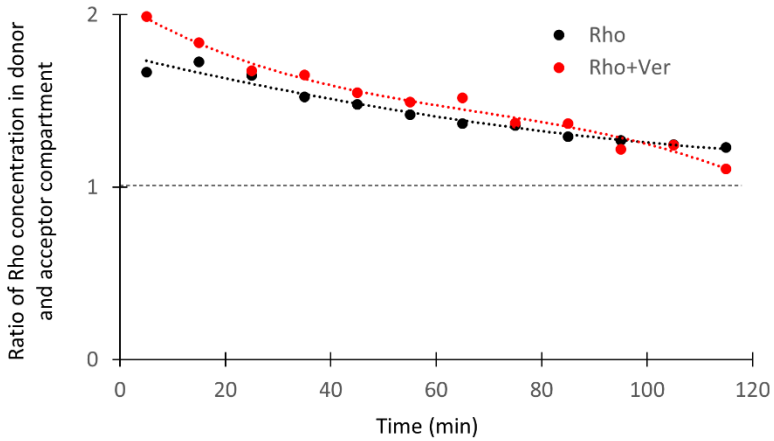

1:10

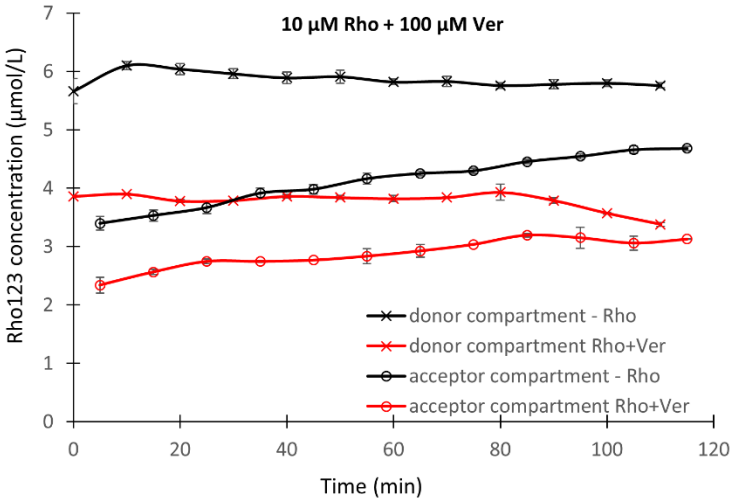

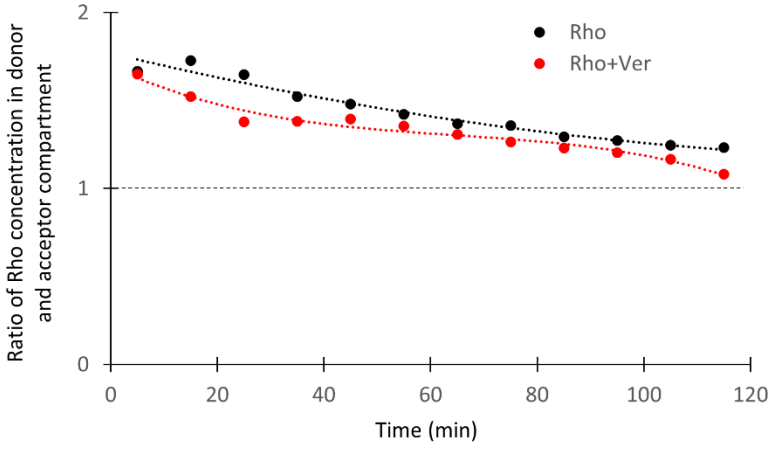

Figure 5

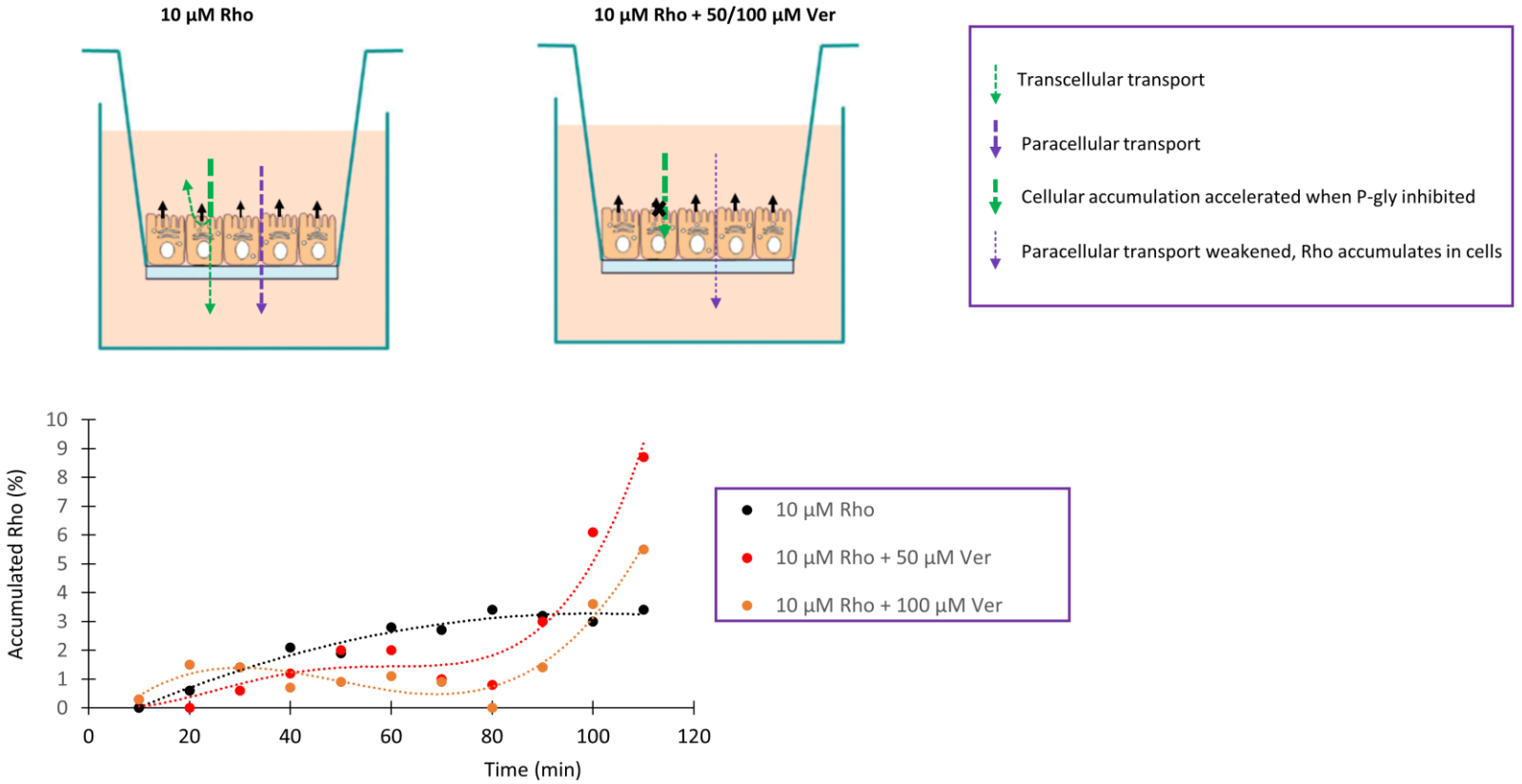
10 µM Rho
10 µM Rho + 50/100 µM Ver
Transcellular transport
Paracellular transport
Cellular accumulation accelerated when P-gly inhibited
Paracellular transport weakened, Rho accumulates in cells
Accumulated Rho (%)
Time (min)
0
20
40
60
80
100
120
1
2
3
4
5
6
7
8
9
10
10 µM Rho
10 µM Rho + 50 µM Ver
10 µM Rho + 100 µM Ver

Figure 6